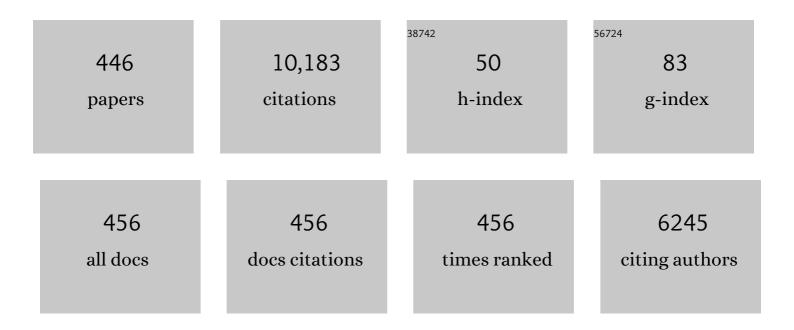
## Takayoshi Nakano

List of Publications by Year in descending order

Source: https://exaly.com/author-pdf/1462155/publications.pdf Version: 2024-02-01



TAKAYOSHI NAKANO

#	Article	IF	CITATIONS
1	Re-Evaluation of Initial Bone Mineralization from an Engineering Perspective. Tissue Engineering - Part B: Reviews, 2022, 28, 246-255.	4.8	3
2	Authors' Response to Letter from Professor Birkedal. Calcified Tissue International, 2022, 110, 144-145.	3.1	2
3	Single crystalline-like crystallographic texture formation of pure tungsten through laser powder bed fusion. Scripta Materialia, 2022, 206, 114252.	5.2	40
4	Design and development of (Ti, Zr, Hf)-Al based medium entropy alloys and high entropy alloys. Materials Chemistry and Physics, 2022, 276, 125409.	4.0	9
5	Bone fragility via degradation of bone quality featured by collagen/apatite micro-arrangement in human rheumatic arthritis. Bone, 2022, 155, 116261.	2.9	14
6	Octacalcium phosphate crystals including a higher density dislocation improve its materials osteogenecity. Applied Materials Today, 2022, 26, 101279.	4.3	13
7	Control of Anisotropic Crystallographic Texture in Powder Bed Fusion Additive Manufacturing of Metals and Ceramics—A Review. Jom, 2022, 74, 1760-1773.	1.9	32
8	Combination treatment with ibandronate and eldecalcitol prevents osteoporotic bone loss and deterioration of bone quality characterized by nano-arrangement of the collagen/apatite in an ovariectomized aged rat model. Bone, 2022, 157, 116309.	2.9	4
9	Periodontal Tissue as a Biomaterial for Hard-Tissue Regeneration following bmp-2 Gene Transfer. Materials, 2022, 15, 993.	2.9	1
10	Ibandronate Suppresses Changes in Apatite Orientation and Young's Modulus Caused by Estrogen Deficiency in Rat Vertebrae. Calcified Tissue International, 2022, 110, 736-745.	3.1	1
11	Improvement of acid resistance of Zn-doped dentin by newly generated chemical bonds. Materials and Design, 2022, 215, 110412.	7.0	4
12	Structural Characterization of Ion Nitrided 316L Austenitic Stainless Steel: Influence of Treatment Temperature and Time. Metals, 2022, 12, 306.	2.3	4
13	Microstructure and mechanical properties of Ti–Nb–Fe–Zr alloys with high strength and low elastic modulus. Transactions of Nonferrous Metals Society of China, 2022, 32, 503-512.	4.2	11
14	Microstructure, mechanical properties, and cytotoxicity of low Young's modulus Ti–Nb–Fe–Sn alloys. Journal of Materials Science, 2022, 57, 5634-5644.	3.7	6
15	Athermal ω Phase and Lattice Modulation in Binary Zr-Nb Alloys. Materials, 2022, 15, 2318.	2.9	1
16	Evaluation of the Microstructural Characteristics of Bone Surrounding Anchor Screws Placed under a Horizontal Load by Exploring the Orientation of Biological Apatite Crystals and Collagen Fiber Anisotropy. Journal of Hard Tissue Biology, 2022, 31, 79-86.	0.4	1
17	Interface characteristics and mechanical behavior of additively manufactured multi-material of stainless steel and Inconel. Materials Science & Engineering A: Structural Materials: Properties, Microstructure and Processing, 2022, 847, 143318.	5.6	11
18	Antibacterial Properties and Biocompatibility of Hydroxyapatite Coating Doped with Various Cu Contents on Titanium. Materials Transactions, 2022, 63, 1072-1079.	1.2	3

#	Article	IF	CITATIONS
19	Additive Manufacturing: Materials, Processing, Characterization and Applications. Crystals, 2022, 12, 747.	2.2	1
20	Outstanding in vivo mechanical integrity of additively manufactured spinal cages with a novel "honeycomb tree structure―design via guiding bone matrix orientation. Spine Journal, 2022, , .	1.3	6
21	Effects of Recrystallization on Tensile Anisotropic Properties for IN738LC Fabricated by Laser Powder Bed Fusion. Crystals, 2022, 12, 842.	2.2	2
22	Equiaxed grain formation by intrinsic heterogeneous nucleation via rapid heating and cooling in additive manufacturing of aluminum-silicon hypoeutectic alloy. Journal of Alloys and Compounds, 2022, 919, 165812.	5.5	21
23	Raking process for Powder Bed Fusion of Ti-6Al-4V alloy Powder Analyzed by Discrete Element Method. Keikinzoku/Journal of Japan Institute of Light Metals, 2022, 72, 291-297.	0.4	1
24	Influence of input energy density on morphology of unique layered microstructure of <i>γ</i> -TiAl alloys fabricated by electron beam powder bed fusion. Keikinzoku/Journal of Japan Institute of Light Metals, 2022, 72, 298-303.	0.4	0
25	A Novel Ex Vivo Bone Culture Model for Regulation of Collagen/Apatite Preferential Orientation by Mechanical Loading. International Journal of Molecular Sciences, 2022, 23, 7423.	4.1	2
26	Development of orthophosphosilicate glass/poly(lactic acid) composite anisotropic scaffolds for simultaneous reconstruction of bone quality and quantity. Journal of Biomedical Materials Research - Part A, 2021, 109, 788-803.	4.0	14
27	Micro/nanostructural Characteristic Changes in the Mandibles of Rats after Injection of Botulinum Neurotoxin. Journal of Hard Tissue Biology, 2021, 30, 183-192.	0.4	1
28	Melting and Solidification Behavior of 316L Steel Induced by Electron-Beam Irradiation for Additive Manufacturing. Journal of Smart Processing, 2021, 10, 208-213.	0.1	2
29	é›»åãf"ãf¼ãf粉末床溶螜³•ã«ã, ã, < Ti-6Al-4V å•́金製ä,‰æ¬¡åfå\$å'質構é€ä½"㮠創製ãëå	¾ॡऀद <u>ऀ</u> 組ç	;1" <b>°</b> ¶å3⁄4;'01
30	Impaired Alignment of Bone Matrix Microstructure Associated with Disorganized Osteoblast Arrangement in Malignant Melanoma Metastasis. Biomolecules, 2021, 11, 131.	4.0	6
31	Effect of Atmosphere Gas on Microstructure in Products of 316L Au stenitic Stainless Steel Fabricated by Laser Powder Bed Fusionï¼^LPBF). Journal of Smart Processing, 2021, 10, 230-234.	0.1	1
32	Ti-6Al-4V ç©å± <b>ë</b> €å½¢ä½"è;¨é¢ä,Šã,ã®ãfŠãfŽã,¢ãf'ã,¿ã,₿f^ã,³ãf¼ãf†ã,£ãf³ã,°ã«ã,^ã,‹ 生体æ′»æ€§èf½ã®	æ"ðå⊢". Jc	our <b>o</b> al of Sma
33	High Precision Manufacturing and Microstructure Control of β-containing γ-TiAl Alloy through Electron Beam Melting. Journal of Smart Processing, 2021, 10, 240-245.	0.1	0
34	レーã,¶ç²‰æœ«åºŠæº¶èžçµå•̂法ã«ã, ̂ã,Šä½œè£½ã⊷㟠Ti-15Mo-5Zr-3Al å•金試料ã«ãŠã'ã,‹æ®‹ç•™a	å¿ <b>œåŠ›ã•ã</b> ,	,¹ã∰f£ãf³ã,1
35	レヹ⁄4ã,¶ç²‰æœ«åºŠæº¶èžçµů•法ã«ã,^ã,‹åºŽé›»æ€§ææ–™ãëã•–ã┥ã®éŠ…å•金ã®é€å¹⁄2¢. Journal of Smart P	roœssing,	2021, 10, 26

36 金属 3D ãf—ãfªãf³ãf†ã,£ãf³ã,°ã«ã,ˆã,‹èj¨é¢æ§‹é€åˆ¶å¾¡ãëãã,Œã«åŸºã¥ãå¹¹ç<sup>°</sup>èfžåˆ¶å¾¡. Journal of Smart Proœssing, 2021, 10, 26

#	Article	IF	CITATIONS
37	Improvement of Mechanical Properties by Microstructural Evolution of Biomedical Co–Cr–W–Ni Alloys with the Addition of Mn and Si. Materials Transactions, 2021, 62, 229-238.	1.2	7
38	Modified Cellular Automaton Simulation of Metal Additive Manufacturing. Nippon Kinzoku Gakkaishi/Journal of the Japan Institute of Metals, 2021, 85, 103-109.	0.4	0
39	Development of TiNbTaZrMo bio-high entropy alloy (BioHEA) super-solid solution by selective laser melting, and its improved mechanical property and biocompatibility. Scripta Materialia, 2021, 194, 113658.	5.2	95
40	Structures and Dissolution Behaviors of Quaternary CaO-SrO-P2O5-TiO2 Glasses. Materials, 2021, 14, 1736.	2.9	6
41	Design and development of Ti–Zr–Hf–Nb–Ta–Mo high-entropy alloys for metallic biomaterials. Materials and Design, 2021, 202, 109548.	7.0	67
42	Surprising increase in yield stress of Mg single crystal using long-period stacking ordered nanoplates. Acta Materialia, 2021, 209, 116797.	7.9	61
43	Influence of Sintering Temperature on Mechanical Properties of Ti-Nb-Zr-Fe Alloys Prepared by Spark Plasma Sintering. Journal of Materials Engineering and Performance, 2021, 30, 5719-5727.	2.5	2
44	Quantitative Evaluation of Osteocyte Morphology and Bone Anisotropic Extracellular Matrix in Rat Femur. Calcified Tissue International, 2021, 109, 434-444.	3.1	25
45	Superior Alignment of Human iPSC-Osteoblasts Associated with Focal Adhesion Formation Stimulated by Oriented Collagen Scaffold. International Journal of Molecular Sciences, 2021, 22, 6232.	4.1	3
46	Unique crystallographic texture formation in Inconel 718 by laser powder bed fusion and its effect on mechanical anisotropy. Acta Materialia, 2021, 212, 116876.	7.9	174
47	Low magnetic field promotes recombinant human BMP-2-induced bone formation and influences orientation of trabeculae and bone marrow-derived stromal cells. Bone Reports, 2021, 14, 100757.	0.4	5
48	Modified Cellular Automaton Simulation of Metal Additive Manufacturing. Materials Transactions, 2021, 62, 864-870.	1.2	6
49	Effect of Precursor Deficiency Induced Ca/P Ratio on Antibacterial and Osteoblast Adhesion Properties of Ag-Incorporated Hydroxyapatite: Reducing Ag Toxicity. Materials, 2021, 14, 3158.	2.9	8
50	Inverse Columnar-Equiaxed Transition (CET) in 304 and 316L Stainless Steels Melt by Electron Beam for Additive Manufacturing (AM). Crystals, 2021, 11, 856.	2.2	20
51	Comparison of Phase Characteristics and Residual Stresses in Ti-6Al-4V Alloy Manufactured by Laser Powder Bed Fusion (L-PBF) and Electron Beam Powder Bed Fusion (EB-PBF) Techniques. Crystals, 2021, 11, 796.	2.2	13
52	Antibacterial Cu-Doped Calcium Phosphate Coating on Pure Titanium. Materials Transactions, 2021, 62, 1052-1055.	1.2	4
53	Improving the Tensile Properties of Additively Manufactured β-Containing TiAl Alloys via Microstructure Control Focusing on Cellular Precipitation Reaction. Crystals, 2021, 11, 809.	2.2	8
54	Development of Low-Yield Stress Co–Cr–W–Ni Alloy by Adding 6 Mass Pct Mn for Balloon-Expandable Stents. Metallurgical and Materials Transactions A: Physical Metallurgy and Materials Science, 2021, 52, 4137-4145.	2.2	4

#	Article	IF	CITATIONS
55	Stability of crystallographic texture in laser powder bed fusion: Understanding the competition of crystal growth using a single crystalline seed. Additive Manufacturing, 2021, 43, 102004.	3.0	27
56	Reduction of Spatter Generation Using Atmospheric Gas in Laser Powder Bed Fusion of Ti–6Al–4V. Materials Transactions, 2021, 62, 1225-1230.	1.2	10
57	Orientation dependence of the wear resistance in the Co–Cr–Mo single crystal. Wear, 2021, 478-479, 203758.	3.1	5
58	3D Puzzle in Cube Pattern for Anisotropic/Isotropic Mechanical Control of Structure Fabricated by Metal Additive Manufacturing. Crystals, 2021, 11, 959.	2.2	17
59	Lattice distortion in selective laser melting (SLM)-manufactured unstable β-type Ti-15Mo-5Zr-3Al alloy analyzed by high-precision X-ray diffractometry. Scripta Materialia, 2021, 201, 113953.	5.2	39
60	Crystallographic texture- and grain boundary density-independent improvement of corrosion resistance in austenitic 316L stainless steel fabricated via laser powder bed fusion. Additive Manufacturing, 2021, 45, 102066.	3.0	17
61	Control of Crystallographic Texture and Mechanical Properties of Hastelloy-X via Laser Powder Bed Fusion. Crystals, 2021, 11, 1064.	2.2	22
62	Comparison of microstructure, crystallographic texture, and mechanical properties in Ti–15Mo–5Zr–3Al alloys fabricated via electron and laser beam powder bed fusion technologies. Additive Manufacturing, 2021, 47, 102329.	3.0	20
63	Structural characteristics of the bone surrounding dental implants placed into the tail-suspended mice. International Journal of Implant Dentistry, 2021, 7, 89.	2.7	3
64	In-air micro-proton-induced X-ray/gamma-ray emission analysis of the acid resistance of root dentin after applying fluoride-containing materials incorporating calcium. Dental Materials Journal, 2021, 40, 1142-1150.	1.8	3
65	Quantitative estimation of kink-band strengthening in an Mg–Zn–Y single crystal with LPSO nanoplates. Materials Research Letters, 2021, 9, 467-474.	8.7	23
66	Fabrication of Ti-Alloy Powder/Solid Composite with Uniaxial Anisotropy by Introducing Unidirectional Honeycomb Structure via Electron Beam Powder Bed Fusion. Crystals, 2021, 11, 1074.	2.2	11
67	Factor which governs the feature of texture developed during additive manufacturing; clarified from the study on hexagonal C40-NbSi2. Scripta Materialia, 2021, 203, 114111.	5.2	15
68	Peculiar microstructural evolution and tensile properties of β-containing γ-TiAl alloys fabricated by electron beam melting. Additive Manufacturing, 2021, 46, 102091.	3.0	21
69	Surface residual stress and phase stability in unstable β-type Ti–15Mo–5Zr–3Al alloy manufactured by laser and electron beam powder bed fusion technologies. Additive Manufacturing, 2021, 47, 102257.	3.0	17
70	Effect of Scan Length on Densification and Crystallographic Texture Formation of Pure Chromium Fabricated by Laser Powder Bed Fusion. Crystals, 2021, 11, 9.	2.2	18
71	Promoting Effect of Basic Fibroblast Growth Factor in Synovial Mesenchymal Stem Cell-Based Cartilage Regeneration. International Journal of Molecular Sciences, 2021, 22, 300.	4.1	8
72	Control of osteoblast arrangement by osteocyte mechanoresponse through prostaglandin E2 signaling under oscillatory fluid flow stimuli. Biomaterials, 2021, 279, 121203.	11.4	20

#	Article	IF	CITATIONS
73	Influence of powder characteristics on densification via crystallographic texture formation: Pure tungsten prepared by laser powder bed fusion. Additive Manufacturing Letters, 2021, 1, 100016.	2.1	14
74	Effect of a helium gas atmosphere on the mechanical properties of Ti-6Al-4V alloy built with laser powder bed fusion: A comparative study with argon gas. Additive Manufacturing, 2021, 48, 102444.	3.0	22
75	Progresses of Additive Manufacturing and Elementary Knowledge of Laser Beam Powder Bed Fusion. Journal of Smart Processing, 2021, 10, 131-136.	0.1	1
76	The combined effects of teriparatide and anti-RANKL monoclonal antibody on bone defect regeneration in ovariectomized mice. Bone, 2020, 130, 115077.	2.9	6
77	Design and fabrication of Ti–Zr-Hf-Cr-Mo and Ti–Zr-Hf-Co-Cr-Mo high-entropy alloys as metallic biomaterials. Materials Science and Engineering C, 2020, 107, 110322.	7.3	105
78	ONO-1301 loaded nanocomposite scaffolds modulate cAMP mediated signaling and induce new bone formation in critical sized bone defect. Biomaterials Science, 2020, 8, 884-896.	5.4	9
79	Selective patterning of netrin-1 as a novel guiding cue for anisotropic dendrogenesis in osteocytes. Materials Science and Engineering C, 2020, 108, 110391.	7.3	13
80	Assessment of the functional efficacy of root canal treatment with high-frequency waves in rats. PLoS ONE, 2020, 15, e0239660.	2.5	3
81	Micro-Architectural Investigation of Teleost Fish Rib Inducing Pliant Mechanical Property. Materials, 2020, 13, 5099.	2.9	5
82	Crystallographic orientation control of pure chromium via laser powder bed fusion and improved high temperature oxidation resistance. Additive Manufacturing, 2020, 36, 101624.	3.0	36
83	ExÂVivo Gene Therapy Treats Bone Complications of Mucopolysaccharidosis Type II Mouse Models through Bone Remodeling Reactivation. Molecular Therapy - Methods and Clinical Development, 2020, 19, 261-274.	4.1	17
84	Using HAADF-STEM for atomic-scale evaluation of incorporation of antibacterial Ag atoms in a β-tricalcium phosphate structure. Nanoscale, 2020, 12, 16596-16604.	5.6	7
85	Impaired bone quality characterized by apatite orientation under stress shielding following fixing of a fracture of the radius with a 3D printed Ti-6Al-4V custom-made bone plate in dogs. PLoS ONE, 2020, 15, e0237678.	2.5	10
86	A Novel Role of Interleukin-6 as a Regulatory Factor of Inflammation-Associated Deterioration in Osteoblast Arrangement. International Journal of Molecular Sciences, 2020, 21, 6659.	4.1	9
87	Microstructure, Mechanical Properties, and Springback of Ti-Nb Alloys Modified by Mo Addition. Journal of Materials Engineering and Performance, 2020, 29, 5366-5373.	2.5	1
88	Control of crystallographic orientation by metal additive manufacturing process of β-type Ti alloys based on the bone tissue anisotropy. MATEC Web of Conferences, 2020, 321, 05002.	0.2	1
89	Low Young's Modulus and High Strength Obtained in Ti-Nb-Zr-Cr Alloys by Optimizing Zr Content. Journal of Materials Engineering and Performance, 2020, 29, 2871-2878.	2.5	6
90	Bone apatite anisotropic structure control <i>via</i> designing fibrous scaffolds. RSC Advances, 2020, 10, 13500-13506.	3.6	16

#	Article	IF	CITATIONS
91	Osteocalcin is necessary for the alignment of apatite crystallites, but not glucose metabolism, testosterone synthesis, or muscle mass. PLoS Genetics, 2020, 16, e1008586.	3.5	119
92	Development of Ti–Zr–Hf–Y–La high-entropy alloys with dual hexagonal-close-packed structure. Scripta Materialia, 2020, 186, 242-246.	5.2	28
93	Micro†and nanoâ€bone analyses of the human mandible coronoid process and tendonâ€bone entheses. Journal of Biomedical Materials Research - Part B Applied Biomaterials, 2020, 108, 2799-2806.	3.4	3
94	Crystallographic Orientation Control of 316L Austenitic Stainless Steel via Selective Laser Melting. ISIJ International, 2020, 60, 1758-1764.	1.4	69
95	Liquid Phase Separation in Ag-Co-Cr-Fe-Mn-Ni, Co Cr-Cu-Fe-Mn-Ni and Co-Cr-Cu-Fe-Mn-Ni-B High Entropy Alloys for Biomedical Application. Crystals, 2020, 10, 527.	2.2	14
96	Combined effect of teriparatide and an anti-RANKL monoclonal antibody on bone defect regeneration in mice with glucocorticoid-induced osteoporosis. Bone, 2020, 139, 115525.	2.9	11
97	Development of Co–Cr–Mo–Fe–Mn–W and Co–Cr–Mo–Fe–Mn–W–Ag High-Entropy Allo Co–Cr–Mo Alloys. Materials Transactions, 2020, 61, 567-576.	ys Based o	on 13
98	Titanium as an Instant Adhesive for Biological Soft Tissue. Advanced Materials Interfaces, 2020, 7, 1902089.	3.7	9
99	Loading Orientation Dependence of the Formation Behavior of Deformation Kink Bands in the Mg-Based Long-Period Stacking Ordered (LPSO) Phase. Materials Transactions, 2020, 61, 821-827.	1.2	8
100	Type I Angiotensin II Receptor Blockade Reduces Uremia-Induced Deterioration of Bone Material Properties. Journal of Bone and Mineral Research, 2020, 36, 67-79.	2.8	11
101	Hypermineralization of Hearing-Related Bones by a Specific Osteoblast Subtype. Journal of Bone and Mineral Research, 2020, 36, 1535-1547.	2.8	9
102	Overexpression of Fam20C in osteoblast in vivo leads to increased cortical bone formation and osteoclastic bone resorption. Bone, 2020, 138, 115414.	2.9	6
103	3D Printing of Anisotropic Bone-Mimetic Structure with Controlled Fluid Flow Stimuli for Osteocytes: Flow Orientation Determines the Elongation of Dendrites. International Journal of Bioprinting, 2020, 6, 293.	3.4	13
104	Analysis of Bone Regeneration Based on the Relationship between the Orientations of Collagen and Apatite in Mouse Femur. Materials Transactions, 2020, 61, 381-386.	1.2	4
105	Effects of unloading by tail suspension on biological apatite crystallite alignment in mouse femur. Dental Materials Journal, 2020, 39, 670-677.	1.8	6
106	Improvement of High Temperature Fatigue Properties of TiAl Alloys Fabricated by Electron Beam Melting Through Hot Isostatic Pressing Process. Journal of Smart Processing, 2020, 9, 180-184.	0.1	2
107	Microstructure and Mechanical Behavior of Ti–25Nb–25Zr Alloy Prepared from Pre-Alloyed and Hydride-Mixed Elemental Powders. Materials Transactions, 2020, 61, 562-566.	1.2	2
108	3D Printing of Biomaterials for Control of Cellular Behaviors. Journal of Smart Processing, 2020, 9, 164-168.	0.1	0

#	Article	IF	CITATIONS
109	Development and Perspectives of High Entropy alloys composed by light metal elements and that for metallic biomaterials with BCC. Keikinzoku/Journal of Japan Institute of Light Metals, 2020, 70, 14-23.	0.4	1
110	Bone Functionalization Based on the Cellular Mechanisms Controlling the Ordered Arrangement of Cells and Bone Matrix Microstructure. Materia Japan, 2020, 59, 594-599.	0.1	0
111	Title is missing!. , 2020, 16, e1008586.		Ο
112	Title is missing!. , 2020, 16, e1008586.		0
113	Title is missing!. , 2020, 16, e1008586.		Ο
114	Title is missing!. , 2020, 16, e1008586.		0
115	Title is missing!. , 2020, 16, e1008586.		Ο
116	Title is missing!. , 2020, 16, e1008586.		0
117	Title is missing!. , 2020, 15, e0237678.		Ο
118	Title is missing!. , 2020, 15, e0237678.		0
119	Title is missing!. , 2020, 15, e0237678.		0
120	Title is missing!. , 2020, 15, e0237678.		0
121	Assessment of the functional efficacy of root canal treatment with high-frequency waves in rats. , 2020, 15, e0239660.		О
122	Assessment of the functional efficacy of root canal treatment with high-frequency waves in rats. , 2020, 15, e0239660.		0
123	Assessment of the functional efficacy of root canal treatment with high-frequency waves in rats. , 2020, 15, e0239660.		Ο
124	Assessment of the functional efficacy of root canal treatment with high-frequency waves in rats. , 2020, 15, e0239660.		0
125	Assessment of the functional efficacy of root canal treatment with high-frequency waves in rats. , 2020, 15, e0239660.		Ο
126	Assessment of the functional efficacy of root canal treatment with high-frequency waves in rats. , 2020, 15, e0239660.		0

#	Article	IF	CITATIONS
127	Radiation-resistant properties of cross-linking PTFE for medical use. Polymer Bulletin, 2019, 76, 6111-6122.	3.3	5
128	Effect of Nb Content on Microstructures and Mechanical Properties of Ti-xNb-2Fe Alloys. Journal of Materials Engineering and Performance, 2019, 28, 5501-5508.	2.5	15
129	Strengthening of Mg-based long-period stacking ordered (LPSO) phase with deformation kink bands. Materials Science & Engineering A: Structural Materials: Properties, Microstructure and Processing, 2019, 763, 138163.	5.6	69
130	Preparation of Titanium Alloy/Bioactive Glass Composite for Biomedical Applications via Selective Laser Melting. Materials Transactions, 2019, 60, 1779-1784.	1.2	6
131	Enhancement of plastic anisotropy and drastic increase in yield stress of Mg-Li single crystals by Al-addition followed by quenching. Scripta Materialia, 2019, 172, 93-97.	5.2	14
132	Development of non-equiatomic Ti-Nb-Ta-Zr-Mo high-entropy alloys for metallic biomaterials. Scripta Materialia, 2019, 172, 83-87.	5.2	124
133	Crystallographic Texture Formation of Pure Tantalum by Selective Laser Melting Method. Journal of Smart Processing, 2019, 8, 151-154.	0.1	5
134	Overcoming the strength-ductility trade-off by the combination of static recrystallization and low-temperature heat-treatment in Co-Cr-W-Ni alloy for stent application. Materials Science & Engineering A: Structural Materials: Properties, Microstructure and Processing, 2019, 766, 138400.	5.6	21
135	Development of bifunctional oriented bioactive glass/poly(lactic acid) composite scaffolds to control osteoblast alignment and proliferation. Journal of Biomedical Materials Research - Part A, 2019, 107, 1031-1041.	4.0	20
136	Biomimetic mineralization using matrix vesicle nanofragments. Journal of Biomedical Materials Research - Part A, 2019, 107, 1021-1030.	4.0	24
137	Physical and mechanical properties of metallic biomaterials. , 2019, , 97-129.		1
138	Quantitative ultrasound (QUS) axial transmission method reflects anisotropy in micro-arrangement of apatite crystallites in human long bones: A study with 3-MHz-frequency ultrasound. Bone, 2019, 127, 82-90.	2.9	16
139	Effect of Oxygen Concentration on the Generation of Spatter during Fabrication via Selective Laser Melting. Journal of Smart Processing, 2019, 8, 102-105.	0.1	4
140	Solidification Microstructures of the Ingots Obtained by Arc Melting and Cold Crucible Levitation Melting in TiNbTaZr Medium-Entropy Alloy and TiNbTaZrX (X = V, Mo, W) High-Entropy Alloys. Entropy, 2019, 21, 483.	2.2	57
141	Unique arrangement of bone matrix orthogonal to osteoblast alignment controlled by Tspan11-mediated focal adhesion assembly. Biomaterials, 2019, 209, 103-110.	11.4	39
142	Oriented siloxane-containing vaterite/poly(lactic acid) composite scaffolds for controlling osteoblast alignment and proliferation. Journal of Asian Ceramic Societies, 2019, 7, 228-237.	2.3	4
143	Development of low-Young's modulus Ti–Nb-based alloys with Cr addition. Journal of Materials Science, 2019, 54, 8675-8683.	3.7	22
144	Additive manufacturing of dense components in beta‑titanium alloys with crystallographic texture from a mixture of pure metallic element powders. Materials and Design, 2019, 173, 107771.	7.0	93

#	Article	IF	CITATIONS
145	UVA-activated riboflavin promotes collagen crosslinking to prevent root caries. Scientific Reports, 2019, 9, 1252.	3.3	21
146	Low Springback and Low Young's Modulus in Ti–29Nb–13Ta–4.6Zr Alloy Modified by Mo Addition. Materials Transactions, 2019, 60, 1755-1762.	1.2	5
147	Effects of Fe on Microstructures and Mechanical Properties of Ti–15Nb–25Zr–(0, 2, 4, 8)Fe Alloys Prepared by Spark Plasma Sintering. Materials Transactions, 2019, 60, 1763-1768.	1.2	5
148	Solidification Microstructure of High Entropy Alloys Composed With 4 Group (Ti, Zr, Hf), 5 Group (V,) Tj ETQq0 C	0 rgBT /C	overlock 10 Ti
149	Excellent mechanical and corrosion properties of austenitic stainless steel with a unique crystallographic lamellar microstructure via selective laser melting. Scripta Materialia, 2019, 159, 89-93.	5.2	267
150	Effects of Autogenous Bone Graft on Mass and Quality of Trabecular Bone in Ti–6Al–4V Spinal Cage Fabricated with Electron Beam Melting. Materials Transactions, 2019, 60, 144-148.	1.2	2
151	Osteoporosis Changes Collagen/Apatite Orientation and Young's Modulus in Vertebral Cortical Bone of Rat. Calcified Tissue International, 2019, 104, 449-460.	3.1	41
152	Beta titanium single crystal with bone-like elastic modulus and large crystallographic elastic anisotropy. Journal of Alloys and Compounds, 2019, 782, 667-671.	5.5	26
153	Synchronous improvement in strength and ductility of biomedical Co–Cr–Mo alloys by unique low-temperature heat treatment. Materials Science & Engineering A: Structural Materials: Properties, Microstructure and Processing, 2019, 739, 53-61.	5.6	16
154	Strengthening mechanisms acting in extruded Mg-based long-period stacking ordered (LPSO)-phase alloys. Acta Materialia, 2019, 163, 226-239.	7.9	200
155	Study on bone quality in the human mandible—Alignment of biological apatite crystallites. Journal of Biomedical Materials Research - Part B Applied Biomaterials, 2019, 107, 838-846.	3.4	5
156	Diffusionless isothermal omega transformation in titanium alloys driven by quenched-in compositional fluctuations. Physical Review Materials, 2019, 3, .	2.4	12
157	Additive Manufacturing of Titanium and Titanium-based Alloys. Materia Japan, 2019, 58, 181-187.	0.1	10
158	Quantitative and Qualitative Relationship between Microstructural Factors and Fatigue Lives under Load- and Strain-Controlled Conditions of Ti–5Al–2Sn–2Zr–4Cr–4Mo (Ti-17) Fabricated Using a 1500-ton Forging Simulator. Materials Transactions, 2019, 60, 1740-1748.	1.2	4
159	Microstructure and Mechanical Properties of TiAl Alloys Prepared by Additive Manufacturing. Journal of Smart Processing, 2019, 8, 78-83.	0.1	1
160	Control of Anisotropic Texture for Improving Creep Property of Nickel Based Superalloy Fabricated by Metal Additive Manufacturing. Journal of Smart Processing, 2019, 8, 106-111.	0.1	1
161	Micro- and Nanostructural Characteristics of Rat Masseter Muscle Entheses. Journal of Hard Tissue Biology, 2019, 28, 365-370.	0.4	5
162	Forefront in Biomedical Materials. Zairyo/Journal of the Society of Materials Science, Japan, 2019, 68, 798-803.	0.2	0

#	Article	IF	CITATIONS
163	Nonâ€surgical model for alveolar bone regeneration by bone morphogenetic proteinâ€2/7 gene therapy. Journal of Periodontology, 2018, 89, 85-92.	3.4	10
164	Microstructure of equiatomic and non-equiatomic Ti-Nb-Ta-Zr-Mo high-entropy alloys for metallic biomaterials. Journal of Alloys and Compounds, 2018, 753, 412-421.	5.5	112
165	Bioinspired Mineralization Using Chondrocyte Membrane Nanofragments. ACS Biomaterials Science and Engineering, 2018, 4, 617-625.	5.2	26
166	Chondrocyte burst promotes space for mineral expansion. Integrative Biology (United Kingdom), 2018, 10, 57-66.	1.3	14
167	Influence of unique layered microstructure on fatigue properties of Ti-48Al-2Cr-2Nb alloys fabricated by electron beam melting. Intermetallics, 2018, 95, 1-10.	3.9	50
168	Novel evaluation method of dentin repair by direct pulp capping using high-resolution micro-computed tomography. Clinical Oral Investigations, 2018, 22, 2879-2887.	3.0	31
169	Effect of scanning strategy on texture formation in Ni-25 at.%Mo alloys fabricated by selective laser melting. Materials and Design, 2018, 140, 307-316.	7.0	222
170	Microstructural Changes During Plastic Deformation and Corrosion Properties of Biomedical Co-20Cr-15W-10Ni Alloy Heat-Treated at 873ÂK. Metallurgical and Materials Transactions A: Physical Metallurgy and Materials Science, 2018, 49, 2393-2404.	2.2	18
171	Effects of single or combination therapy of teriparatide and anti-RANKL monoclonal antibody on bone defect regeneration in mice. Bone, 2018, 106, 1-10.	2.9	16
172	Plastic deformation mechanisms of biomedical Co–Cr–Mo alloy single crystals with hexagonal close-packed structure. Scripta Materialia, 2018, 142, 111-115.	5.2	24
173	Construction of human induced pluripotent stem cellâ€derived oriented bone matrix microstructure by using <i>in vitro</i> engineered anisotropic culture model. Journal of Biomedical Materials Research - Part A, 2018, 106, 360-369.	4.0	40
174	Trabecular health of vertebrae based on anisotropy in trabecular architecture and collagen/apatite micro-arrangement after implantation of intervertebral fusion cages in the sheep spine. Bone, 2018, 108, 25-33.	2.9	24
175	Strain-rate dependence of deformation behavior of LPSO-phases. Materials Letters, 2018, 214, 119-122.	2.6	12
176	Low Young's Modulus Ti–Nb–O with High Strength and Good Plasticity. Materials Transactions, 2018, 59, 858-860.	1.2	9
177	Dynamic Collision Behavior Between Osteoblasts and Tumor Cells Regulates the Disordered Arrangement of Collagen Fiber/Apatite Crystals in Metastasized Bone. International Journal of Molecular Sciences, 2018, 19, 3474.	4.1	14
178	Effects of Heat Treatment on Unique Layered Microstructure and Tensile Properties of TiAl Fabricated by Electron Beam Melting. Materials Science Forum, 2018, 941, 1366-1371.	0.3	12
179	Rapid bioinspired mineralization using cell membrane nanofragments and alkaline milieu. Journal of Materials Chemistry B, 2018, 6, 6153-6161.	5.8	15
180	Quantitative Analysis of the Preferential Orientation of Collagen and Elastin Fibers in Blood Vessel with an Imaging Methodology Combined with Birefringence Measurement. Nippon Kinzoku Gakkaishi/Journal of the Japan Institute of Metals, 2018, 82, 64-69.	0.4	0

#	Article	IF	CITATIONS
181	Strategy for Construction of Anisotropic Bone Matrix by Using Biomedical Materials. Kobunshi Ronbunshu, 2018, 75, 164-173.	0.2	0
182	Ϊ‰-phase transformation and lattice modulation in biomedical β-phase Ti-Nb-Al alloys. Journal of Alloys and Compounds, 2018, 766, 511-516.	5.5	18
183	Dual release of growth factor from nanocomposite fibrous scaffold promotes vascularisation and bone regeneration in rat critical sized calvarial defect. Acta Biomaterialia, 2018, 78, 36-47.	8.3	85
184	A paradigm shift for bone quality in prosthetic dentistry. Annals of Japan Prosthodontic Society, 2018, 10, 1-15.	0.0	0
185	Effects of long-term cigarette smoke exposure on bone metabolism, structure, and quality in a mouse model of emphysema. PLoS ONE, 2018, 13, e0191611.	2.5	26
186	Design and Development of Intervertebral Fusion Cage with Novel Concept by Metal Powder-Based Additive Manufacturing. Funtai Oyobi Fummatsu Yakin/Journal of the Japan Society of Powder and Powder Metallurgy, 2018, 65, 132-134.	0.2	0
187	Creation of Anisotropic Properties by Morphology and Microstructure Control in the Additive Manufactured Metallic Materials. Materia Japan, 2018, 57, 145-149.	0.1	2
188	Crystallographic Texture Formation of Beta-type Ti-15Mo-5Zr-3Al Alloy Through Selective Laser Melting. Journal of Smart Processing, 2018, 7, 229-232.	0.1	12
189	Activity Report from the 4th Sectional Committee on the Delegation Program for Young Researchers to Medical and Dental Conferences. Materia Japan, 2018, 57, 504-506.	0.1	0
190	Crystallographic orientation of the c-axis of biological apatite as a new index of the quality of subchondral bone in knee joint osteoarthritis. Journal of Bone and Mineral Metabolism, 2017, 35, 308-314.	2.7	13
191	Successful additive manufacturing of MoSi2 including crystallographic texture and shape control. Journal of Alloys and Compounds, 2017, 696, 67-72.	5.5	66
192	Synchronous disruption of anisotropic arrangement of the osteocyte network and collagen/apatite in melanoma bone metastasis. Journal of Structural Biology, 2017, 197, 260-270.	2.8	57
193	Disruption of collagen/apatite alignment impairs bone mechanical function in osteoblastic metastasis induced by prostate cancer. Bone, 2017, 97, 83-93.	2.9	69
194	Preparation of orthophosphate glasses in the MgO–CaO–SiO2–Nb2O5–P2O5 system. Bio-Medical Materials and Engineering, 2017, 28, 23-30.	0.6	3
195	Development of unique cross-lamellar microstructure, resulting in the drastic increase in fracture toughness in Cr/Ir-codoped (Mo 0.85 Nb 0.15 )Si 2 crystals. Scripta Materialia, 2017, 131, 19-23.	5.2	5
196	Crystallographic texture control of beta-type Ti–15Mo–5Zr–3Al alloy by selective laser melting for the development of novel implants with a biocompatible low Young's modulus. Scripta Materialia, 2017, 132, 34-38.	5.2	302
197	Molecular level analyses of mechanical properties of PTFE sterilized by Co-60 Î <sup>3</sup> -ray irradiation for clinical use. Radiation Physics and Chemistry, 2017, 139, 126-131.	2.8	11
198	Biocompatible nanostructured solid adhesives for biological soft tissues. Acta Biomaterialia, 2017, 57, 404-413.	8.3	25

#	Article	IF	CITATIONS
199	Development of a root canal treatment model in the rat. Scientific Reports, 2017, 7, 3315.	3.3	40
200	Alteration of osteoblast arrangement via direct attack by cancer cells: New insights into bone metastasis. Scientific Reports, 2017, 7, 44824.	3.3	38
201	Use of PIXE/PIGE for sequential Ca and F measurements in root carious model. Scientific Reports, 2017, 7, 13450.	3.3	10
202	Unusual dynamic precipitation softening induced by dislocation glide in biomedical beta-titanium alloys. Scientific Reports, 2017, 7, 8056.	3.3	9
203	Co-deteriorations of anisotropic extracellular matrix arrangement and intrinsic mechanical property in c-src deficient osteopetrotic mouse femur. Bone, 2017, 103, 216-223.	2.9	35
204	Structure, dissolution behavior, cytocompatibility, and antibacterial activity of silver ontaining calcium phosphate invert glasses. Journal of Biomedical Materials Research - Part A, 2017, 105, 3127-3135.	4.0	17
205	Influences of scanning speed and short-time heat treatment on fundamental properties of Ti-6Al-4V alloy produced by EBM method. Materials Science & Engineering A: Structural Materials: Properties, Microstructure and Processing, 2017, 704, 246-251.	5.6	20
206	A paradigm shift for bone quality in dentistry: A literature review. Journal of Prosthodontic Research, 2017, 61, 353-362.	2.8	36
207	Unloading-Induced Degradation of the Anisotropic Arrangement of Collagen/Apatite in Rat Femurs. Calcified Tissue International, 2017, 100, 87-94.	3.1	44
208	Experimental clarification of the cyclic deformation mechanisms of β-type Ti–Nb–Ta–Zr-alloy single crystals developed for the single-crystalline implant. International Journal of Plasticity, 2017, 98, 27-44.	8.8	25
209	Outstanding compressive creep strength in Cr/Ir-codoped (Mo0.85Nb0.15)Si2 crystals with the unique cross-lamellar microstructure. Scientific Reports, 2017, 7, 3936.	3.3	3
210	Optimally oriented grooves on dental implants improve bone quality around implants under repetitive mechanical loading. Acta Biomaterialia, 2017, 48, 433-444.	8.3	45
211	Novel TiNbTaZrMo high-entropy alloys for metallic biomaterials. Scripta Materialia, 2017, 129, 65-68.	5.2	262
212	Formation and structural analysis of 15MgO–15CaO–8P2O5–4SiO2 glass. Journal of Non-Crystalline Solids, 2017, 457, 73-76.	3.1	16
213	Effect of building direction on the microstructure and tensile properties of Ti-48Al-2Cr-2Nb alloy additively manufactured by electron beam melting. Additive Manufacturing, 2017, 13, 61-70.	3.0	148
214	Alignment of Biological Apatite Crystallites in Peri-Implant Bone of Beagles. Materials Transactions, 2017, 58, 107-112.	1.2	2
215	Control of Morphological and Microstructural Anisotropy through Powder-Based Metal Additive Manufacturing. Funtai Oyobi Fummatsu Yakin/Journal of the Japan Society of Powder and Powder Metallurgy, 2017, 64, 259-264.	0.2	0
216	Effects of mechanical repetitive load on bone quality around implants in rat maxillae. PLoS ONE, 2017, 12, e0189893.	2.5	29

#	Article	IF	CITATIONS
217	Design of the Next Generation Metallic Biomaterials. Materia Japan, 2017, 56, 584-588.	0.1	2
218	Fundamentals of Metal 3D Printing Technologies. Materia Japan, 2017, 56, 686-690.	0.1	20
219	Impaired Bone Matrix Alignment Induced by Breast Cancer Metastasis. Nippon Kinzoku Gakkaishi/Journal of the Japan Institute of Metals, 2017, 81, 308-314.	0.4	Ο
220	Association between Intraosseous Vasculature and Bone Matrix Anisotropy Analyzed with a Novel Visualization Method. Nippon Kinzoku Gakkaishi/Journal of the Japan Institute of Metals, 2017, 81, 315-319.	0.4	0
221	Directional Control of Mature Osteoblast Derived from Juvenile Mouse Calvariae. Materials Transactions, 2017, 58, 958-962.	1.2	2
222	Structural Crosstalk between Crystallographic Anisotropy in Bone Tissue and Vascular Network Analyzed with a Novel Visualization Method. Materials Transactions, 2017, 58, 266-270.	1.2	4
223	Transition and Prospect of Biomedical and Healthcare Materials from the Viewpoint of Tissue Regeneration. Materia Japan, 2017, 56, 220-224.	0.1	0
224	Preferential Arrangement of Mature Osteoblast from Juvenile Mouse Calvariae on the Oriented Collagen Substrate. Nippon Kinzoku Gakkaishi/Journal of the Japan Institute of Metals, 2017, 81, 480-484.	0.4	0
225	Special Issue on Advances in Biomedical Materials Science and Technology. Materials Transactions, 2016, 57, 1985-1985.	1.2	0
226	Control of Cellular Arrangement by Surface Topography Induced by Plastic Deformation. Crystals, 2016, 6, 73.	2.2	10
227	Biological Apatite Crystallite Alignment Analysis of Human Maxillary Molar Region Cortical Bone with Microbeam X-ray Diffraction. Journal of Hard Tissue Biology, 2016, 25, 109-114.	0.4	1
228	Influence of Implant Neck Design on Bone Formation Under Mechanical Repetitive Loading. Implant Dentistry, 2016, 25, 171-178.	1.3	2
229	Anomalous strengthening behavior of Co–Cr–Mo alloy single crystals for biomedical applications. Scripta Materialia, 2016, 123, 149-153.	5.2	30
230	<i>In vitro</i> assessment of a calcium-fluoroaluminosilicate glass-based desensitizer for the prevention of root surface demineralization. Dental Materials Journal, 2016, 35, 399-407.	1.8	14
231	Comprehensive analyses of how tubule occlusion and advanced glycation end-products diminish strength of aged dentin. Scientific Reports, 2016, 6, 19849.	3.3	63
232	Ϊ‰ Phase Transformation and Mechanical Properties in Binary Zr-Nb Biomedical Alloy. Materials Science Forum, 2016, 879, 1969-1973.	0.3	1
233	Induction of Biological Apatite Orientation as a Bone Quality Parameter in Bone Regeneration Using Hydroxyapatite/Poly É>-Caprolactone Composite Scaffolds. Tissue Engineering - Part C: Methods, 2016, 22, 856-863.	2.1	5
234	High-Temperature Deformation Behavior of (Mo <sub>0.85</sub> Nb <sub>0.15</sub> )Si <sub>2</sub> Crystals with C40/C11 <sub>b</sub> Lamellar Microstructure. Materials Science Forum, 2016, 879, 677-683.	0.3	1

#	Article	IF	CITATIONS
235	Isotropic plasticity of β-type Ti-29Nb-13Ta-4.6Zr alloy single crystals for the development of single crystalline β-Ti implants. Scientific Reports, 2016, 6, 29779.	3.3	21
236	Development of Custom Lighting Device by Additive Manufacturing Technology with Metal Powder. Funtai Oyobi Fummatsu Yakin/Journal of the Japan Society of Powder and Powder Metallurgy, 2016, 63, 82-84.	0.2	0
237	Development of Anatomical Plate for Fracture Treatment of Companion Animal by EBM Method. Funtai Oyobi Fummatsu Yakin/Journal of the Japan Society of Powder and Powder Metallurgy, 2016, 63, 85-87.	0.2	0
238	Development of Customized Bone Plate for Companion Animal. Materia Japan, 2016, 55, 64-66.	0.1	0
239	Development of Metal Customized Illumination by Additive Manufacturing Technology Based on the Delight Design. Materia Japan, 2016, 55, 18-20.	0.1	0
240	Alignment of Biological Apatite c-Axis Under Functional Loading. Implant Dentistry, 2016, 25, 594-598.	1.3	4
241	Effect of additional elements on fracture toughness of (Mo0.85Nb0.15)Si2 C40/C11b lamellar-structured crystals. Materials Letters, 2016, 177, 99-103.	2.6	7
242	Electron backscatter diffraction pattern analysis of the deformation band formed in the Mg-based long-period stacking ordered phase. Scripta Materialia, 2016, 117, 32-36.	5.2	34
243	Microstructure and fracture toughness in boron added NbSi2(C40)/MoSi2(C11b) duplex crystals. Scripta Materialia, 2016, 113, 236-240.	5.2	29
244	Crystal-orientation-dependent corrosion behaviour of single crystals of a pure Mg and Mg-Al and Mg-Cu solid solutions. Corrosion Science, 2016, 109, 68-85.	6.6	123
245	Plastic deformation behavior of 10H-type synchronized LPSO phase in a Mg–Zn–Y system. Acta Materialia, 2016, 109, 90-102.	7.9	112
246	Creep-deformation behavior of (Mo0.85Nb0.15)Si2 lamellar-structured C40/C11b two-phase crystals. Acta Materialia, 2016, 107, 196-212.	7.9	28
247	Orientation dependence of the deformation kink band formation behavior in Zn single crystal. International Journal of Plasticity, 2016, 77, 174-191.	8.8	76
248	Elastic-modulus enhancement during room-temperature aging and itsÂsuppression in metastable Ti–Nb-Based alloys with low body-centered cubic phase stability. Acta Materialia, 2016, 102, 373-384.	7.9	50
249	Evaluation of crystallographic orientation of biological apatite in vertebral cortical bone in ovariectomized cynomolgus monkeys treated with minodronic acid and alendronate. Journal of Bone and Mineral Metabolism, 2016, 34, 234-241.	2.7	22
250	Disruption of Collagen Matrix Alignment in Osteolytic Bone Metastasis Induced by Breast Cancer. Materials Transactions, 2016, 57, 2077-2082.	1.2	9
251	Fluorescent Imaging of Cell Arrangement Controlled by Materials Scientific Techniques. Materia Japan, 2016, 55, 579-579.	0.1	1
252	Experimental and computational approaches for the understanding of the nature of deformation band formed in materials with hexagonal crystal structures. The Proceedings of the Materials and Mechanics Conference, 2016, 2016, OS01-11.	0.0	0

#	Article	IF	CITATIONS
253	Motivations and Concepts for Our SIP Program on "Establishment and Validation of the Base for 3D Design & Additive Manufacturing Standing on the Concept "Anisotropy" & "Customization" ". Materia Japan, 2015, 54, 496-497.	0.1	0
254	Control of "Material Parameters" and "Structural Parameters" for Anisotropic and Customized Design. Materia Japan, 2015, 54, 502-504.	0.1	0
255	Preface to Special Issue on "Establishment and Validation of the Base for 3D Design & Additive Manufacturing Standing on the Concept "Anisotropy" & "Customization" ". Materia Japan, 2015, 54, 491-492.	0.1	0
256	Delight Assessment of Anisotropic Custom Plate. Materia Japan, 2015, 54, 515-516.	0.1	0
257	Solid/Powder Clad Ti-6Al-4V Alloy with Low Young's Modulus and High Toughness Fabricated by Electron Beam Melting. Materials Transactions, 2015, 56, 755-758.	1.2	5
258	In-Situ Observation on the Formation Behavior of the Deformation Kink Bands in Zn Single Crystal and LPSO Phase. Materials Transactions, 2015, 56, 943-951.	1.2	38
259	An Approach to Creation of Innovation Styles for Anisotropic and Customized Design and Manufacture. Materia Japan, 2015, 54, 519-521.	0.1	Ο
260	Formation of Crystallographic Orientation of Bone Apatite Crystallites Investigated by Powder-Metallurgical Method and Development of Novel Bone Implant Focusing on Apatite Orientation. Funtai Oyobi Fummatsu Yakin/Journal of the Japan Society of Powder and Powder Metallurgy, 2015, 62, 580-586.	0.2	1
261	Structural and Qualitative Bone Remodeling Around Repetitive Loaded Implants in Rabbits. Clinical Implant Dentistry and Related Research, 2015, 17, e699-710.	3.7	21
262	Alignment of Biological Apatite Crystallites in Posterior Cortical Bone of Human Edentulous Mandible. Journal of Hard Tissue Biology, 2015, 24, 235-240.	0.4	5
263	Development of Single Crystalline Bone Plate with Low Young's Modulus Using Beta-type Ti-15Mo-5Zr-3Al Alloy. Tetsu-To-Hagane/Journal of the Iron and Steel Institute of Japan, 2015, 101, 501-505.	0.4	4
264	Powder-based Additive Manufacturing for Development of Tailor-made Implants for Orthopedic Applications. KONA Powder and Particle Journal, 2015, 32, 75-84.	1.7	42
265	Quantitative regulation of boneâ€mimetic, oriented collagen/apatite matrix structure depends on the degree of osteoblast alignment on oriented collagen substrates. Journal of Biomedical Materials Research - Part A, 2015, 103, 489-499.	4.0	82
266	Crystallographic nature of deformation bands shown in Zn and Mg-based long-period stacking ordered (LPSO) phase. Philosophical Magazine, 2015, 95, 132-157.	1.6	49
267	Altered material properties are responsible for bone fragility in rats with chronic kidney injury. Bone, 2015, 81, 247-254.	2.9	45
268	Stochastic multi-scale prediction on the apparent elastic moduli of trabecular bone considering uncertainties of biological apatite (BAp) crystallite orientation and image-based modelling. Computer Methods in Biomechanics and Biomedical Engineering, 2015, 18, 162-174.	1.6	15
269	Novel powder/solid composites possessing low Young's modulus and tunable energy absorption capacity, fabricated by electron beam melting, for biomedical applications. Journal of Alloys and Compounds, 2015, 639, 336-340.	5.5	40
270	Combination of BMP-2-releasing gelatin/ $\hat{l}^2$ -TCP sponges with autologous bone marrow for bone regeneration of X-ray-irradiated rabbit ulnar defects. Biomaterials, 2015, 56, 18-25.	11.4	53

#	Article	IF	CITATIONS
271	Mechanisms of lamellar structure formation and Cr interfacial segregation in C11b-MoSi2/C40-NbSi2 dual phase silicide verified by a phase-field simulation incorporating elastic inhomogeneity. Computational Materials Science, 2015, 108, 358-366.	3.0	8
272	Early Initiation of Endochondral Ossification of Mouse Femur Cultured in Hydrogel with Different Mechanical Stiffness. Tissue Engineering - Part C: Methods, 2015, 21, 567-575.	2.1	12
273	Clinical efficacy and safety of monthly oral ibandronate 100Âmg versus monthly intravenous ibandronate 1Âmg in Japanese patients with primary osteoporosis. Osteoporosis International, 2015, 26, 2685-2693.	3.1	21
274	Abnormal arrangement of a collagen/apatite extracellular matrix orthogonal to osteoblast alignment is constructed by a nanoscale periodic surface structure. Biomaterials, 2015, 37, 134-143.	11.4	102
275	Bone Tissue and Biomaterial Design Based on the Anisotropic Microstructure. Springer Series in Biomaterials Science and Engineering, 2015, , 3-30.	1.0	6
276	Mechanisms of Cr segregation to C11b/C40 lamellar interface in (Mo,Nb)Si2 duplex silicide: A phase-field study to bridge experimental and first-principles investigations. Intermetallics, 2014, 54, 232-241.	3.9	12
277	Promotion of Endodontic Lesions in Rats by a Novel Extraradicular Biofilm Model Using Obturation Materials. Applied and Environmental Microbiology, 2014, 80, 3804-3810.	3.1	17
278	Misfit analysis in lamellar microstructure in NbSi2/MoSi2 duplex crystals. Journal of Alloys and Compounds, 2014, 607, 48-49.	5.5	3
279	Dietary L-Lysine Prevents Arterial Calcification in Adenine-Induced Uremic Rats. Journal of the American Society of Nephrology: JASN, 2014, 25, 1954-1965.	6.1	47
280	Degradation behavior of Ca–Mg–Zn intermetallic compounds for use as biodegradable implant materials. Materials Science and Engineering C, 2014, 44, 285-292.	7.3	16
281	Control of Mechanical Properties of Three-Dimensional Ti-6Al-4V Products Fabricated by Electron Beam Melting with Unidirectional Elongated Pores. Metallurgical and Materials Transactions A: Physical Metallurgy and Materials Science, 2014, 45, 4293-4301.	2.2	31
282	<i>Ab-initio</i> study of long-period superstructures and anti-phase boundaries in Al-rich <i>γ</i> -TiAl (L1 <sub>0</sub> )-based alloys. Philosophical Magazine, 2014, 94, 1202-1218.	1.6	7
283	Control of microstructure and fracture toughness improvement of NbSi2/MoSi2 duplex lamellar silicides by TaC particles dispersion. Scripta Materialia, 2014, 82, 53-56.	5.2	10
284	Development of Metal Bio-functional Materials by Additive Manufacturing. Journal of Smart Processing, 2014, 3, 167-174.	0.1	1
285	In vivo Corrosion Environment and Biomaterials. Zairyo To Kankyo/ Corrosion Engineering, 2014, 63, 290-294.	0.2	1
286	Mesenchymal stromal cells improve the osteogenic capabilities of mineralized agarose gels in a rat full-thickness cranial defect model. Journal of Tissue Engineering and Regenerative Medicine, 2013, 7, 51-60.	2.7	13
287	Degree of biological apatite <i>c</i> -axis orientation rather than bone mineral density controls mechanical function in bone regenerated using recombinant bone morphogenetic protein-2. Journal of Bone and Mineral Research, 2013, 28, 1170-1179.	2.8	144
288	Possibility of Mg- and Ca-based intermetallic compounds as new biodegradable implant materials. Materials Science and Engineering C, 2013, 33, 4101-4111.	7.3	27

#	Article	IF	CITATIONS
289	Advanced Analysis and Control of Bone Microstructure Based on a Materials Scientific Study Including Microbeam X-ray Diffraction. , 2013, , 155-167.		4
290	Long-period ordered superstructures that appear in an (Al,Ga)-rich (Al,Ga)Ti system. Philosophical Magazine, 2013, 93, 22-37.	1.6	0
291	Formation of <i>c</i> -axis-oriented columnar structures through controlled epitaxial growth of hydroxyapatite. Journal of Asian Ceramic Societies, 2013, 1, 143-148.	2.3	15
292	Non-basal slip in Ni3(Ti, Nb) and Ni3(Ti, Al) single crystals with various long-period stacking ordered structures. Acta Materialia, 2013, 61, 4365-4373.	7.9	4
293	Individual mechanical properties of ferrite and martensite in Fe–0.16mass% C–1.0mass% Si–1.5mass% Mn steel. Journal of Alloys and Compounds, 2013, 577, S593-S596.	5.5	20
294	Misfit strain affecting the lamellar microstructure in NbSi2/MoSi2 duplex crystals. Acta Materialia, 2013, 61, 3432-3444.	7.9	29
295	Continuous cyclic stretch induces osteoblast alignment and formation of anisotropic collagen fiber matrix. Acta Biomaterialia, 2013, 9, 7227-7235.	8.3	87
296	ω Transformation in cold-worked Ti–Nb–Ta–Zr–O alloys with low body-centered cubic phase stability and its correlation with their elastic properties. Acta Materialia, 2013, 61, 139-150.	7.9	78
297	Design and optimization of the oriented groove on the hip implant surface to promote bone microstructure integrity. Bone, 2013, 52, 659-667.	2.9	78
298	Yield stress anomaly controlled by the phase stability in NbSi2 single crystals. Scripta Materialia, 2013, 68, 313-316.	5.2	12
299	Cr segregation at C11b/C40 interface in MoSi2-based alloys: A first-principles study. Intermetallics, 2013, 42, 165-169.	3.9	14
300	Phase-Field Study on the Segregation Mechanism of Additive Elements in NbSi2/MoSi2 Duplex Silicide. Materials Research Society Symposia Proceedings, 2013, 1516, 145-150.	0.1	4
301	Phase-Field Simulation of Lamellar Structure Formation in MoSi2/NbSi2 Duplex Silicide. Materials Research Society Symposia Proceedings, 2013, 1516, 309-315.	0.1	4
302	First-principles investigation of phase stability and electronic structure of tetragonal (P4/m) Ga <sub>3â~²</sub> <i><sub>x</sub></i> Al <i><sub>x</sub></i> Ti <sub>2</sub> ( <i>x</i> = 0–3) com Philosophical Magazine Letters, 2013, 93, 273-282.	pauends.	1
303	Uncertainty Modeling in the Prediction of Effective Mechanical Properties Using Stochastic Homogenization Method with Application to Porous Trabecular Bone. Materials Transactions, 2013, 54, 1250-1256.	1.2	16
304	^ ^beta;-Phase Instability and Effects on the Physical Properties in Binary Ti-Nb Biomaterial Single Crystals. Nippon Kinzoku Gakkaishi/Journal of the Japan Institute of Metals, 2013, 77, 281-286.	0.4	2
305	Preferential Orientation of Collagen/Biological Apatite in Growing Rat Ulna under an Artificial Loading Condition. Materials Transactions, 2013, 54, 1257-1261.	1.2	6
306	Conditions for Osteoblast Arrangement Induced under Long-Term Cyclic Stretching. Materials Transactions, 2013, 54, 1195-1199.	1.2	2

#	Article	IF	CITATIONS
307	β-Phase Instability in Binary Ti– <i>x</i> Nb Biomaterial Single Crystals. Materials Transactions, 2013, 54, 156-160.	1.2	16
308	Non-Basal Slip Systems Operative in Mg <sub>12</sub> ZnY Long-Period Stacking Ordered (LPSO) Phase with 18R and 14H Structures. Materials Transactions, 2013, 54, 693-697.	1.2	57
309	Relationship between Preferential Alignment of Biological Apatite and Young^ ^rsquo;s Modulus at First Molar in Human Mandible Cortical Bone. Journal of Hard Tissue Biology, 2013, 22, 163-170.	0.4	6
310	Alignment of Biological Apatite Crystallites at First Molar in Human Mandible Cortical Bone. Cranio - Journal of Craniomandibular Practice, 2012, 30, 32-40.	1.4	14
311	First-principles study on phase stability of MoSi <mml:math xmlns:mml="http://www.w3.org/1998/Math/MathML" display="inline"&gt;<mml:msub><mml:mrow /&gt;<mml:mn>2</mml:mn></mml:mrow </mml:msub>-NbSi<mml:math xmlns:mml="http://www.w3.org/1998/Math/MathML" display="inline"&gt;<mml:msub><mml:mrow< td=""><td>3.2</td><td>6</td></mml:mrow<></mml:msub></mml:math </mml:math 	3.2	6
312	b cmm/mmv2 c/mm/mmv c/mm/msub> c/mm/math>pseudobinary alloys. Physical Review 8, 2012, 85, . Effects of a coating resin containing S-PRG filler to prevent demineralization of root surfaces. Dental Materials Journal, 2012, 31, 909-915.	1.8	62
313	Analysis of Biological Apatite Crystal Orientation in Anterior Cortical Bone of Human Mandible Using Microbeam X-ray Diffractometry. Materials Transactions, 2012, 53, 980-984.	1.2	13
314	Bone Loss and Degradation of Bone Quality in the Human Femur after Total Hip Arthroplasty under Stress-Shielding by Titanium-Based Implant. Nippon Kinzoku Gakkaishi/Journal of the Japan Institute of Metals, 2012, 76, 468-473.	0.4	2
315	Bone Loss and Reduced Bone Quality of the Human Femur after Total Hip Arthroplasty under Stress-Shielding Effects by Titanium-Based Implant. Materials Transactions, 2012, 53, 565-570.	1.2	91
316	The alignment of MC3T3-E1 osteoblasts on steps of slip traces introduced by dislocation motion. Biomaterials, 2012, 33, 7327-7335.	11.4	81
317	Biological apatite (BAp) crystallographic orientation and texture as a new index for assessing the microstructure and function of bone regenerated by tissue engineering. Bone, 2012, 51, 741-747.	2.9	107
318	Biocompatible low Young's modulus achieved by strong crystallographic elastic anisotropy in Ti–15Mo–5Zr–3Al alloy single crystal. Journal of the Mechanical Behavior of Biomedical Materials, 2012, 14, 48-54.	3.1	110
319	Morphology analysis of vertebral trabecular bone under dynamic loading based on multi-scale theory. Medical and Biological Engineering and Computing, 2012, 50, 1091-1103.	2.8	11
320	Chronological histological changes during bone regeneration on a non-crosslinked atelocollagen matrix. Journal of Bone and Mineral Metabolism, 2012, 30, 638-650.	2.7	9
321	In vitro reproduction of endochondral ossification using a 3D mesenchymal stem cell construct. Integrative Biology (United Kingdom), 2012, 4, 1207.	1.3	43
322	The preparation of PLLA/calcium phosphate hybrid composite and its evaluation of biocompatibility. Dental Materials Journal, 2012, 31, 1087-1096.	1.8	12
323	Microstructural and Orientation Dependence of the Plastic Deformation Behavior in Î <sup>2</sup> -type Ti-15Mo-5Zr-3Al Alloy Single Crystals. Metallurgical and Materials Transactions A: Physical Metallurgy and Materials Science, 2012, 43, 1588-1597.	2.2	23
324	Optimization of Cr content of metastable β-type Ti–Cr alloys with changeable Young's modulus for spinal fixation applications. Acta Biomaterialia, 2012, 8, 2392-2400.	8.3	107

#	Article	IF	CITATIONS
325	7B34 Evaluation of apatite orientation as a bone quality parameter in regenerative and diseased bone and the related mechanical property The Proceedings of the Bioengineering Conference Annual Meeting of BED/JSME, 2012, 2012.24, _7B34-17B34-2	0.0	0
326	Design of Biomaterials for Bone Replacement Based on Parameters Determining Bone Quality. , 2012, , 55-65.		1
327	OS0306 Kink deformation in synchronized LPSO-phase and HCP metals. The Proceedings of the Materials and Mechanics Conference, 2012, 2012, _OS0306-1OS0306-2	0.0	1
328	Effects of Cr-addition and lamellar microstructure on the oxidation behavior of single crystal (Mo0.85Nb0.15)Si2. Journal of Alloys and Compounds, 2011, 509, 1511-1516.	5.5	1
329	Numerical Study on the Morphology and Mechanical Role of Healthy and Osteoporotic Vertebral Trabecular Bone. Journal of Biomechanical Science and Engineering, 2011, 6, 270-285.	0.3	13
330	Plastic Deformation Behavior of Mg <sub>12</sub> ZnY LPSO-Phase with 14H-Typed Structure. Materials Transactions, 2011, 52, 1096-1103.	1.2	98
331	Development of high Zr-containing Ti-based alloys with low Young's modulus for use in removable implants. Materials Science and Engineering C, 2011, 31, 1436-1444.	7.3	113
332	Zirconia–hydroxyapatite composite material with micro porous structure. Dental Materials, 2011, 27, e205-e212.	3.5	40
333	Low Young's modulus in Ti–Nb–Ta–Zr–O alloys: Cold working and oxygen effects. Acta Materialia, 2011, 59, 6975-6988.	7.9	122
334	Biomechanical evaluation of regenerating long bone by nanoindentation. Journal of Materials Science: Materials in Medicine, 2011, 22, 969-976.	3.6	50
335	Fracture behavior and toughness of NbSi2-based single crystals and MoSi2(C11b)/NbSi2(C40) duplex crystals with a single set of lamellae. Acta Materialia, 2011, 59, 4168-4176.	7.9	33
336	Monte Carlo simulation of antiphase boundaries and growth of antiphase domains in Al <sub>5</sub> Ti <sub>3</sub> phase in Al-rich γ-TiAl intermetallics. Philosophical Magazine, 2011, 91, 3068-3078.	1.6	4
337	Cell-Based Fabrication of Organic/Inorganic Composite Gel Material. Materials, 2011, 4, 327-338.	2.9	5
338	Formation of New Bone with Preferentially Oriented Biological Apatite Crystals Using a Novel Cylindrical Implant Containing Anisotropic Open Pores Fabricated by the Electron Beam Melting (EBM) Method. ISIJ International, 2011, 51, 262-268.	1.4	29
339	Regenerative behavior of biomineral/agarose composite gels as bone grafting materials in rat cranial defects. Journal of Biomedical Materials Research - Part A, 2010, 93A, 965-975.	4.0	23
340	Proliferation and osteogenic differentiation of rat bone marrow stromal cells on bioapatite with different crystalline facets. Journal of Biomedical Materials Research - Part A, 2010, 93A, 646-655.	4.0	3
341	Structure and Mechanical Properties of Melt-Extracted Beta-Ti-Type Ti-Nb-Ta-Zr (TNTZ) Wire with High Bending Ductility. Nippon Kinzoku Gakkaishi/Journal of the Japan Institute of Metals, 2010, 74, 515-519.	0.4	0
342	Fabrication of Beta-Ti-Type Ti-Nb-Ta-Zr (TNTZ) Wire with High-Ductility by Arc-Melt-Type Melt-Extraction Method. Materials Transactions, 2010, 51, 377-380.	1.2	0

#	Article	IF	CITATIONS
343	Proliferation and differentiation potential of pluripotent mesenchymal precursor C2C12 cells on resin-based restorative materials. Dental Materials Journal, 2010, 29, 341-346.	1.8	19
344	Improvement of aligned lamellar structure by Cr-addition to NbSi2/MoSi2 duplex–silicide crystals. Scripta Materialia, 2010, 62, 613-616.	5.2	23
345	Low Young's modulus of Ti–Nb–Ta–Zr alloys caused by softening in shear moduli c′ and c44 near lower limit of body-centered cubic phase stability. Acta Materialia, 2010, 58, 6790-6798.	7.9	90
346	Changes of Bone Quality and Quantity in rhM-CSF-Treated Osteopetrotic (op/op) Mice. Materials Science Forum, 2010, 654-656, 2249-2252.	0.3	0
347	Evaluation of Mechanical Properties of Regenerated Bone by Nanoindentation Technique. Materials Science Forum, 2010, 654-656, 2220-2224.	0.3	1
348	Change in Biological Apatite Orientation in Beagle Mandible. Materials Science Forum, 2010, 654-656, 2216-2219.	0.3	8
349	Evaluation and Control of Crystallographic Alignment of Biological Apatite Crystallites in Bones. Materials Science Forum, 2010, 654-656, 2212-2215.	0.3	0
350	Quantity and Quality of Regenerated Bone in Grooves Aligned at Different Angles from the Implant Surface. Materials Science Forum, 2010, 654-656, 2241-2244.	0.3	4
351	Effect of Calcium Ion Concentrations on Osteogenic Differentiation and Hematopoietic Stem Cell Niche-Related Protein Expression in Osteoblasts. Tissue Engineering - Part A, 2010, 16, 2467-2473.	3.1	127
352	Plastic deformation behavior of Ni3(Ti0.7Nb0.3) single crystals with D019 structure. Intermetallics, 2010, 18, 434-440.	3.9	3
353	Formation and development of C40/C11b lamellar structure in NbSi2/MoSi2 crystals. Intermetallics, 2010, 18, 2328-2332.	3.9	4
354	Efficacy of polyphasic calcium phosphates as a direct pulp capping material. Journal of Dentistry, 2010, 38, 828-837.	4.1	24
355	Analysis of Biological Apatite Orientation in Rat Mandibles. Oral Science International, 2010, 7, 19-25.	0.7	9
356	In vitro engineering of transitional tissue by patterning and functional control of cells in fibrin gel. Soft Matter, 2010, 6, 1662.	2.7	9
357	Formation of New Bone with Preferentially Oriented Biological Apatite Crystals Using Novel Cylindrical Implant Containing Anisotropic Open Pores Fabricated by Electron Beam Melting (EBM) Method. Tetsu-To-Hagane/Journal of the Iron and Steel Institute of Japan, 2010, 96, 572-578.	0.4	3
358	1302 Visualization of Load Bearing Function of Trabeculae in Vertebra under Various Mechanical Conditions. The Proceedings of the Materials and Mechanics Conference, 2010, 2010, 351-353.	0.0	0
359	The combination therapy with alfacalcidol and risedronate improves the mechanical property in lumbar spine by affecting the material properties in an ovariectomized rat model of osteoporosis. BMC Musculoskeletal Disorders, 2009, 10, 66.	1.9	39
360	Effect of spatial design and thermal oxidation on apatite formation on Ti–15Zr–4Ta–4Nb alloy. Acta Biomaterialia, 2009, 5, 298-304.	8.3	52

#	Article	IF	CITATIONS
361	Chemical-Hydrothermal Synthesis of Bioinert ZrO <sub>2</sub> -TiO <sub>2</sub> Films on Pure Ti Substrates and Proliferation of Osteoblast-Like Cells. Materials Transactions, 2009, 50, 2147-2153.	1.2	8
362	Fabrication of Ti-Zr Binary Metallic Wire by Arc-Melt-Type Melt-Extraction Method. Materials Transactions, 2009, 50, 872-878.	1.2	7
363	Oxygen Distribution in Titanium Single Crystal Fabricated by Optical Floating-Zone Method under Extremely Low Oxygen Partial Pressure. Materials Transactions, 2009, 50, 2709-2715.	1.2	6
364	Microscopic Properties of Long-Period Ordering in Al-Rich TiAl Alloys. Metallurgical and Materials Transactions A: Physical Metallurgy and Materials Science, 2008, 39, 1610-1617.	2.2	10
365	Alendronate treatment promotes bone formation with a less anisotropic microstructure during intramembranous ossification in rats. Journal of Bone and Mineral Metabolism, 2008, 26, 24-33.	2.7	42
366	Peculiar elastic behavior of Ti–Nb–Ta–Zr single crystals. Acta Materialia, 2008, 56, 2856-2863.	7.9	220
367	Effects of antiphase domains on dislocation motion in Ti <sub>3</sub> Al single crystals deformed by prism slip. Philosophical Magazine, 2008, 88, 465-488.	1.6	20
368	Multimodal joint attention through cross facilitative learning based on $\hat{l}^1\!\!\!/ \!\!\!/ X$ principle. , 2008, , .		11
369	Preferential orientation of biological apatite crystallite in original, regenerated and diseased cortical bones. Journal of the Ceramic Society of Japan, 2008, 116, 313-315.	1.1	10
370	New Technique for Evaluation of Preferential Alignment of Biological Apatite (BAp) Crystallites in Bone Using Transmission X-ray Diffractometry. Materials Transactions, 2008, 49, 2129-2135.	1.2	18
371	Effects of the anisotropy of the anti-phase boundary energy on the yield-stress anomaly in Ni3Xcompounds with close-packed crystal structures. Philosophical Magazine Letters, 2007, 87, 705-712.	1.2	6
372	Areal Distribution of Preferential Alignment of Biological Apatite (BAp) Crystallite on Cross-Section of Center of Femoral Diaphysis in Osteopetrotic (op/op) Mouse. Materials Transactions, 2007, 48, 337-342.	1.2	33
373	Two-Dimensional Quantitative Analysis of Preferential Alignment of BAp c-axis for Isolated Human Trabecular Bone Using Microbeam X-ray Diffractometer with a Transmission Optical System. Materials Transactions, 2007, 48, 343-347.	1.2	28
374	Construction of 3D Morphology Model Based on CT-images and Mechanical Analysis Based on Elastic Anisotropy Caused by Crystallographic Orientation of Biological Apatite in Trabecular Bone. Materia Japan, 2007, 46, 834-834.	0.1	0
375	Plastic deformation behavior of NbSi2/MoSi2 crystals with oriented lamellae. Intermetallics, 2006, 14, 1345-1350.	3.9	32
376	Evaluation of Bone Quality near Metallic Implants with and without Lotus-Type Pores for Optimal Biomaterial Design. Materials Transactions, 2006, 47, 2233-2239.	1.2	34
377	Martensitic Transformation Behavior and Shape Memory Properties of Ti–Ni–Pt Melt-Spun Ribbons. Materials Transactions, 2006, 47, 540-545.	1.2	6
378	Effect of C11b-Stabilized Element on Deformation Mode in C40-Type (Nb1-xMox)Si2 (x=0-0.85) Single Crystals. Materials Research Society Symposia Proceedings, 2006, 980, 2.	0.1	0

#	Article	IF	CITATIONS
379	Effects of Al concentration and resulting long-period superstructures on the plastic properties at room temperature of Al-rich TiAl single crystals. Philosophical Magazine, 2005, 85, 2527-2548.	1.6	15
380	Long-period ordering in a TiAl single crystal with a gradient composition. Philosophical Magazine Letters, 2005, 85, 175-185.	1.2	9
381	Texture and Bone Reinforcement. , 2005, , 1-8.		26
382	Texture of Biological Apatite Crystallites and the Related Mechanical Function in Regenerated and Pathological Hard Tissues. Journal of Hard Tissue Biology, 2005, 14, 363-364.	0.4	6
383	Dislocation Structure and Yield Stress Anomaly in D0 <sub>24</sub> Ni <sub>3</sub> Ti Compounds withthe GCP Structure. Materia Japan, 2005, 44, 997-997.	0.1	0
384	Effects of long-period superstructures on plastic properties in Al-rich TiAl single crystals. Materials Research Society Symposia Proceedings, 2004, 842, 501.	0.1	2
385	Transformation Behavior of TiNiPt Thin Films Fabricated Using Melt Spinning Technique. Materials Research Society Symposia Proceedings, 2004, 842, 144.	0.1	6
386	Crystal Structure, Phase Stability and Plastic Deformation Behavior of Ti-rich Ni3(Ti, Nb) Single Crystals with Various Long-Period Ordered Structures Materials Research Society Symposia Proceedings, 2004, 842, 25.	0.1	0
387	Indentation fracture behavior of (Mo0.85Nb0.15)Si2crystals with C40 single-phase and MoSi2(C11b)/NbSi2(C40) duplex-phase with oriented lamellae. Science and Technology of Advanced Materials, 2004, 5, 11-17.	6.1	21
388	EFFECTS OF APPLIED STRESS ON PREFERENTIAL ALIGNMENT OF BIOLOGICAL APATITE IN RABBIT FORELIMB BONES. Phosphorus Research Bulletin, 2004, 17, 77-82.	0.6	13
389	ANALYSIS OF PREFERENTIAL ALIGNMENT OF BIOLOGICAL APATITE CRYSTALLITES IN SUBCHONDRAL BONE OF THE OSTEOARTHRITIC KNEE. Phosphorus Research Bulletin, 2004, 17, 83-84.	0.6	6
390	Stacking Structure and Phase Stability in Ni-based GCP Compounds. Materia Japan, 2004, 43, 993-993.	0.1	0
391	Preferential Alignment of c-axis of Biological Apatite in Trabecular Bone. Materia Japan, 2004, 43, 1032-1032.	0.1	0
392	Effect of Rh and V Additions on Plastic Deformation Behaviour in Ni <sub>3</sub> Nb Single Crystals with D0 <sub>a</sub> Structure. Materials Transactions, 2002, 43, 2267-2274.	1.2	3
393	Effect of Antiphase Domain Boundaries on Prism Slip in Ti3Al Single Crystals. Materials Research Society Symposia Proceedings, 2002, 753, 1.	0.1	2
394	HRTEM Observation of Partially Ordered Long-Period Superstructures in Al-Rich TiAl Alloys. Materials Research Society Symposia Proceedings, 2002, 753, 1.	0.1	1
395	Plastic Deformation Behavior of Al5Ti3 Single-Phase Single Crystals. Materials Research Society Symposia Proceedings, 2002, 753, 1.	0.1	1
396	Formation and stability of transitional long-period superstructures in Al-rich Ti-Al single crystals. Philosophical Magazine A: Physics of Condensed Matter, Structure, Defects and Mechanical Properties, 2002, 82, 763-777.	0.6	27

#	Article	IF	CITATIONS
397	Unique alignment and texture of biological apatite crystallites in typical calcified tissues analyzed by microbeam x-ray diffractometer system. Bone, 2002, 31, 479-487.	2.9	330
398	Microstructure and compressive flow stress of directionally solidified ternary Ni3(Al, Nb) and quaternary Ni3(Al, Nb, Ti) alloys with duplexphase. Science and Technology of Advanced Materials, 2002, 3, 193-199.	6.1	7
399	Variation in crystallinity of hydroxyapatite and the related calcium phosphates by mechanical grinding and subsequent heat treatment. Metallurgical and Materials Transactions A: Physical Metallurgy and Materials Science, 2002, 33, 521-528.	2.2	34
400	Selection and change in deformation mode to maintain continuity of strains and slip/twinning planes at lamellar boundaries in fatigued TiAl polysynthetically twinned crystals. Science and Technology of Advanced Materials, 2002, 3, 225-237.	6.1	2
401	Microstructure of duplex-phase NbSi2(C40)/MoSi2(C11b) crystals containing a single set of lamellae. Acta Materialia, 2002, 50, 1781-1795.	7.9	61
402	Plastic deformation behaviour and deformation substructure in Al-rich TiAl single crystals deformed at high temperatures. Science and Technology of Advanced Materials, 2001, 2, 433-441.	6.1	10
403	Plastic Deformation by Slip on (001)[100] in Ni <sub>3</sub> Nb Single Crystals with D0 <sub>a</sub> Structure. Materials Transactions, 2001, 42, 1998-2002.	1.2	8
404	Control of hydroxyapatite crystallinity by mechanical grinding method. Journal of Materials Science: Materials in Medicine, 2001, 12, 703-706.	3.6	18
405	Classification of γ-γ and γ-α2lamellar boundaries on the basis of continuity of strains and slip-twinning planes in fatigued TiAl polysynthetically twinned crystals. Philosophical Magazine A: Physics of Condensed Matter, Structure, Defects and Mechanical Properties, 2001, 81, 1447-1471.	0.6	15
406	Classification of Î <sup>3</sup> -Î <sup>3</sup> and Î <sup>3</sup> -α2 lamellar boundaries on the basis of continuity of strains and slip-twinning planes in fatigued TiAl polysynthetically twinned crystals. Philosophical Magazine A: Physics of Condensed Matter, Structure, Defects and Mechanical Properties, 2001, 81, 1447-1471.	0.6	2
407	Anomalous Strengthening Mechanism in NbSi2-Based Silicide Single Crystals. Materials Research Society Symposia Proceedings, 2000, 646, 56.	0.1	0
408	Deformation Twins in Ni3Nb Single Crystals with DOa Structure. Materials Research Society Symposia Proceedings, 2000, 646, 68.	0.1	3
409	Microstructure and Plastic Deformation in Unidirectionally Solidified NbSi2 (C40) /MoSi2 (C11b) Crystals. Materials Research Society Symposia Proceedings, 2000, 646, 377.	0.1	0
410	Effect of substitutational elements on plastic deformation behaviour of NbSi2-based silicide single crystals with C40 structure. Acta Materialia, 2000, 48, 3465-3475.	7.9	47
411	Deformation Substructure in Ni <sub>3</sub> Nb Single Crystals with the D0 <sub>a</sub> Structure. Materia Japan, 2000, 39, 996-996.	0.1	0
412	Effect of deformation temperature on fatigue and fracture behavior in TiAl polysynthetically twinned crystals. Metallurgical and Materials Transactions A: Physical Metallurgy and Materials Science, 1998, 29, 943-950.	2.2	0
413	Effect of deformation temperature on fatigue and fracture behavior in TiAl polysynthetically twinned crystals. Metallurgical and Materials Transactions A: Physical Metallurgy and Materials Science, 1998, 29, 943-950.	2.2	10
414	Microstructure and high-temperature strength in duplex silicides. Intermetallics, 1998, 6, 715-722.	3.9	52

#	Article	IF	CITATIONS
415	Effect of A12Ti Phase on Plastic Behavior in Ti-62.5at%Al Single Crystals. Materials Research Society Symposia Proceedings, 1998, 552, 1.	0.1	3
416	Plastic Deformation of Ni3Nb Single Crystals. Materials Research Society Symposia Proceedings, 1998, 552, 1.	0.1	3
417	Dislocation Structure in Ti <sub>3</sub> Al Single Crystals Cyclically Deforming by Prism Slip. Materia Japan, 1998, 37, 363-363.	0.1	0
418	Fatigue, Cyclic Deformation and Microstructure. Plastic Deformation Behaviour and Substructure in CoTi Single Crystals Fatigued at Room Temperature ISIJ International, 1997, 37, 1218-1223.	1.4	3
419	Development of multi channel neutron spectrometer at GEKKO XII laser fusion facility. AIP Conference Proceedings, 1996, , .	0.4	2
420	The deformation substructure in cyclically deformed TiAl PST crystals. Philosophical Magazine A: Physics of Condensed Matter, Structure, Defects and Mechanical Properties, 1996, 73, 1035-1051.	0.6	12
421	Effect of chemical ordering on the deformation mode of Al-rich Ti-Al single crystals. Philosophical Magazine A: Physics of Condensed Matter, Structure, Defects and Mechanical Properties, 1996, 74, 251-268.	0.6	45
422	Effect of lamellar structure and plastic anisotropy on the cyclic deformation and fatigue behaviour of TiAl PST crystals. Philosophical Magazine A: Physics of Condensed Matter, Structure, Defects and Mechanical Properties, 1996, 73, 1053-1067.	0.6	10
423	Cold-rolling and Recovery Behaviours of Ti3Al Single Crystals with D019 Structure ISIJ International, 1996, 36, 111-120.	1.4	6
424	Cyclic deformation behaviour of Ti-Al alloys containing oriented lamellae. Philosophical Magazine A: Physics of Condensed Matter, Structure, Defects and Mechanical Properties, 1995, 71, 127-138.	0.6	25
425	Effect of Addition of .BETAPhase Stabilizing Elements(Nb, Mo and V) on Plastic Behaviour of Ti3Al Single Crystals with the D019 Structure ISIJ International, 1995, 35, 900-907.	1.4	7
426	Plastic Behavior and Deformation Structure of Silicide Single Crystals with Transition Metals at High Temperatures. Materials Research Society Symposia Proceedings, 1993, 322, 9.	0.1	22
427	The role of ordered domains and slip mode of α2 phase in the plastic behaviour of TiAl crystals containing oriented lamellae. Acta Metallurgica Et Materialia, 1993, 41, 1155-1161.	1.8	122
428	Deformation behavior and high-temperature stability of unidirectionally solidified, twin phase TiAl. Journal of Materials Research, 1993, 8, 1812-1816.	2.6	0
429	Plastic Anisotropy of Ti3Al Single Crystals. Materials Research Society Symposia Proceedings, 1992, 288, 441.	0.1	17
430	Plastic Behaviour of TiAl Crystals Containing a Single Set of Lamellae at High Temperatures ISIJ International, 1992, 32, 1339-1347.	1.4	55
431	Fabrication and Characterization of Porous Implant Products with Aligned Pores by EBM Method for Biomedical Application. Advanced Materials Research, 0, 409, 142-145.	0.3	7
432	Hydrothermal Modification of Products Fabricated by Electron Beam Melting. Key Engineering Materials, 0, 529-530, 580-583.	0.4	0

#	Article	IF	CITATIONS
433	Control of Osteoblastic Cell Behavior by Surface Topography Introduced by Plastic Deformation of Ti Single Crystal with h.c.p. Structure. Materials Science Forum, 0, 706-709, 549-552.	0.3	0
434	Assessment of the Elastic Properties of Human Femoral Bone with Artificial Hip Joint by Ultrasound Transmission. Key Engineering Materials, 0, 529-530, 321-324.	0.4	0
435	Evaluation of Bone Quality in Mandible of Young M-CSF Deficient-Induced Osteopetrotic Mouse. Materials Science Forum, 0, 706-709, 484-487.	0.3	0
436	Effect of Energy Density of Incident Beam on Mechanical Property of Titanium Alloy Products Fabricated by Electron Beam Melting (EBM) Method. Materials Science Forum, 0, 706-709, 488-491.	0.3	6
437	Single Crystal Growth and its Microstructure in Co-Cr-Mo Alloys for Biomedical Applications. Materials Science Forum, 0, 706-709, 561-565.	0.3	2
438	Regeneration of Bone Mass and Bone Quality around Implant with Grooves for Aligning Bone Cells in Rabbit Hindlimb Bones. Materials Science Forum, 0, 706-709, 510-513.	0.3	0
439	Interface Migration with Segregation in MoSi <sub>2</sub> -Based Lamellar Alloy Simulated by Phase-Field Method. Advanced Materials Research, 0, 922, 832-837.	0.3	3
440	Development of a New Powder/Solid Composite for Biomimic Implant Materials by Electron-Beam Additive Manufacturing. Materials Science Forum, 0, 879, 1361-1364.	0.3	8
441	Fabrication of the Beta-Titanium Alloy Rods from a Mixture of Pure Metallic Element Powders via Selected Laser Melting. Materials Science Forum, 0, 941, 1260-1263.	0.3	6
442	Microstructure and Fatigue Properties of TiAl with Unique Layered Microstructure Fabricated by Electron Beam Melting. Materials Science Forum, 0, 941, 1597-1602.	0.3	10
443	Improvement of Strength and Ductility by Combining Static Recrystallization and Unique Heat Treatment in Co-20Cr-15W-10Ni Alloy for Stent Application. Materials Science Forum, 0, 1016, 1503-1509.	0.3	0
444	Fabrication of Be-Ta Ti Alloys without Pre-Alloyed Powders via SLM. Materials Science Forum, 0, 1016, 1797-1801.	0.3	0
445	Novel Ti–Zr–Hf–Nb–Ta–Mo High-Entropy Alloys for Metallic Biomaterials. SSRN Electronic Journal, 0, , .	0.4	1
446	Microstructure, Mechanical Properties, and Cytotoxicity of β-Type Ti-Nb-Cr Alloys Designed by Electron Parameter. Journal of Materials Engineering and Performance, 0, , 1.	2.5	1